2008 IEEE International Conference on
Robotics and Automation
Pasadena, CA, USA, May 19-23, 2008

Kinematic Calibration of a 7-DOF Self-Calibrated Modular Cable-Driven Robotic Arm

Shabbir Kurbanhusen Mustafa, *Student Member, IEEE,* Guilin Yang, *Member, IEEE,* Song Huat Yeo, and Wei Lin, *Member, IEEE*

***Abstract*— This paper presents the kinematic calibration of a novel 7-degree-of-freedom (DOF) cable-driven robotic arm (CDRA), aimed at improving its absolute positioning accuracy. This CDRA consists of three 'self-calibrated' cable-driven parallel mechanism (CDPM) modules. In order to account for any kinematic errors that might arise when assembling the individual CDPMs, a calibration model is formulated based on the local product-of-exponential formula and the measurement residues in the tool-tip frame poses. An iterative least-squares algorithm is employed to identify the errors in the fixed transformation frames of the sequentially assembled 'self-calibrated' CDPM modules. Both computer simulations and experimental studies were carried out to verify the robustness and effectiveness of the proposed calibration algorithm. From the experimental studies, errors in the fixed kinematic transformation frames were precisely recovered after a minimum of 15 pose measurements.**

I. INTRODUCTION

The advancement of robotics technology in recent years has led to robots being increasingly introduced into daily human activities. These robots co-exist alongside humans and even cooperate with humans in daily tasks to enhance the quality of life. There has been a long research focus in humanoid robots to develop lightweight dexterous robotic arms that are functionally similar to the human arm [1]. The focus has mainly been on the development of robotic arms, as these arms will come in direct contact with the human body. Hence, in order for these robots to successfully work, cooperate and interact with humans, they must be designed to have intrinsically safe features.

Based on the various applications such as service robots [1], [2], human-machine interface devices [3], and robotic rehabilitation devices [4], [5], numerous robotic arms resembling the human arm have been designed. The most common humanoid arm design is a 7-DOF serial articulated manipulator with its joint actuators mounted onto the arm itself. While most of these robotic arms possess several fundamental features of the human arm, the mechanism design and driving scheme of these arms are still different from the human arm. As a result, such robotics arms are intrinsically dangerous due to their heavy mechanical structure and large moment of inertia.

This work was partially supported by Nanyang Technological University under Academic Research Fund RG 24/06.

S.K. Mustafa, G. Yang and W. Lin are with the Mechatronics Group, Singapore Institute of Manufacturing Technology, Singapore 638075. {mustafa,glyang,wlin}@simtech.a-star.edu.sg

S.H. Yeo is with the School of Mechanical & Aerospace Engineering, Nanyang Technological University, Singapore 639798. myeosh@ntu.edu.sg

In order to address the above-mentioned shortcomings, a novel 'biologically-inspired' design for a humanoid robotic arm was proposed in [6] based on observations made on the human arm anatomical structure. The result is a 7-DOF cable-driven robotic arm (CDRA) that consists of three sequentially connected cable-driven parallel mechanism (CDPM) modules, i.e., a 3-DOF CDPM shoulder module, a 1-DOF CDPM elbow module, and a 3-DOF CDPM wrist module. A robotic arm research prototype was subsequently developed (see Fig. 1), which is lightweight ($\approx$ 1 kilogram) for intrinsically-safe manipulation, and possesses the essential features of a human arm such as high redundancy, a large reachable workspace, and high dexterity.

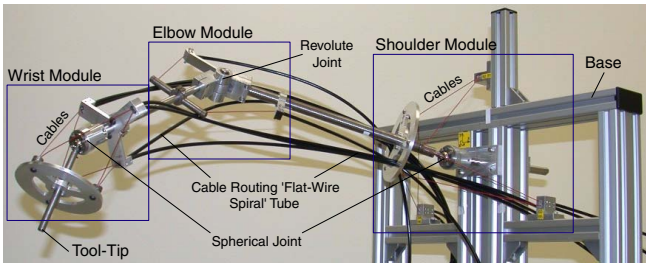

Fig. 1. Research prototype of the biologically-inspired 7-DOF cable-driven robotic arm (CDRA)

For path planning and motion control tasks, the accuracy of the geometric model parameters greatly influence the positioning accuracy of the end-effector [7]. Geometric model parameters deviate from their nominal values due to manufacturing tolerance, compliance, wear of connecting mechanisms and link misalignments. In addition, this robotic arm consists of several modular cable-driven parallel mechanisms that are sequentially assembled to form the overall 7-DOF cable-driven robotic arm. Cables by nature are flexible and they introduce compliancy which further reduces the positional accuracy. This will result in larger assembly errors as compared to rigid-linked robotic arms with fixed configurations. Hence, calibration must be carried out to minimize these sources of inaccuracy.

For the 7-DOF cable-driven robotic arm, the complete calibration procedure is divided into two progressive stages (see Fig. 2). The first stage is the self-calibration of the various CDPM modules, and the second stage is the calibration of the 7-DOF CDRA assembly. Self-calibration is carried out to calibrate the kinematic model of each CDPM module by using the redundant cable length information.

Calibration, on the other hand, is carried out to identify the fixed kinematic transformations between the inertial base frame, the assembled CDPM modules, and the tool-tip frame, by using external pose measurement devices. It is aimed at improving the absolute positioning accuracy of the robotic arm.

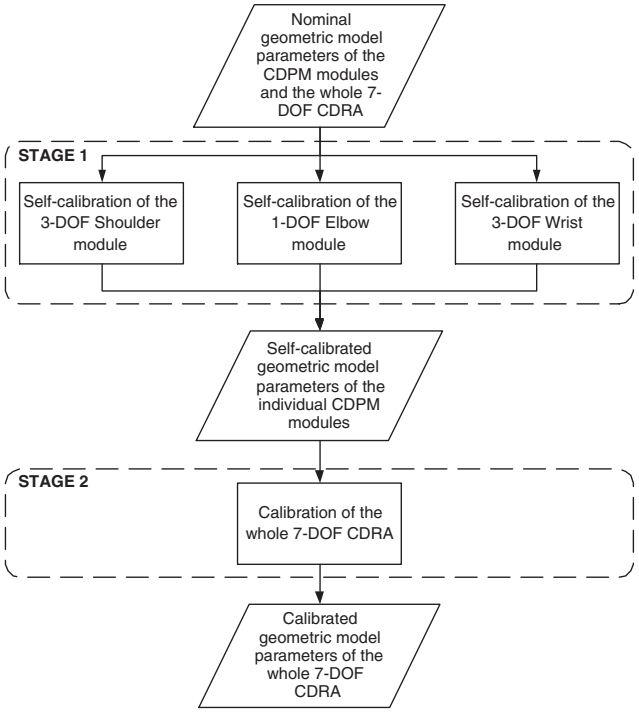

Fig. 2. Flowchart of the calibration procedure from the individual CDPM modules to the complete 7-DOF CDRA

The success of the calibration stage is greatly dependent on the accuracy of the kinematic models of the individual CDPM modules obtained from the self-calibration stage. Self-calibration of the individual CDPM modules has been addressed in [8] and this paper will focus on the calibration of the assembled 7-DOF CDRA to minimize errors introduced during assembly. This is based on previous experimental studies in which the individual CDPM modules have undergone self-calibration, and their individual kinematic models can be computed with sufficient accuracy.

One of the early works to address the fixed kinematic transformation calibration of robotic systems was by Zhuang [9]. In this work, a linear solution based on the quaternion algebra was proposed. This approach allowed simultaneous computation of the fixed kinematic transformation, which is fast and non-iterative. However, this approach suffered from formulation singularity problem which meant that several arrangements of the fixed kinematic transformation frames had to be avoided. This calibration issue was also addressed by Yang [10]. In this work, the calibration problem was cast into an iterative parameter identification process using the *product-of-exponential* (POE) formula. The basic idea was to treat the errors in the fixed kinematic transformations as a twist, i.e., an element of *se(3)*. Because a twist has a 6-dimensional vector representation, the formulation is simplified and it does not suffer any formulation singularity problem. While the approach in [10] addressed the calibration of a self-calibrated modular parallel robot, this approach is extended in this paper to address the calibration of a 7-DOF self-calibrated modular cable-driven robotic arm.

The next few sections will present the assembled 7-DOF CDRA calibration methodology, including the kinematic modeling of the CDRA, the calibration model and the calibration algorithm. This will be followed by computer simulation examples and experimental studies to validate the accuracy and robustness of the proposed calibration model.

II. KINEMATIC MODEL DESCRIPTION

The kinematic model of the whole 7-DOF cable-driven robotic arm is described by a world coordinate frame $\{K_O\}$, and the respective base and moving platform coordinate frames of the individual CDPM modules (see Fig. 3).

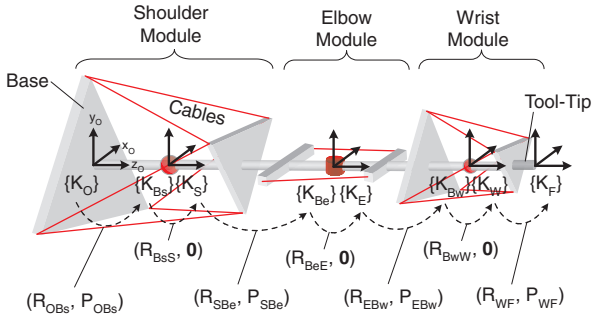

Fig. 3. Kinematic model of the optimized 7-DOF CDRA

The forward kinematic transformation of the tool-tip coordinate frame $\{K_F\}$ relative to the world coordinate frame $\{K_O\}$ is given as:

$$\mathbf{T}_{OF} = \mathbf{T}_{OB_s}.\mathbf{T}_{B_sS}.\mathbf{T}_{SB_e}.\mathbf{T}_{B_eE}.\mathbf{T}_{EB_w}.\mathbf{T}_{B_wW}.\mathbf{T}_{WF} \qquad (1)$$

Where transformation matrices $\mathbf{T}_{OB_s}$, $\mathbf{T}_{SB_e}$, $\mathbf{T}_{EB_w}$ and $\mathbf{T}_{WF}$ are fixed forward kinematic transformations between the various modules attached serially to form the 7-DOF CDRA (i.e., from the moving platform frames of the individual CDPMs to the base frames of the previous modules attached in series). Transformation matrices $\mathbf{T}_{B_sS}$, $\mathbf{T}_{B_eE}$ and $\mathbf{T}_{B_wW}$ are the forward kinematic transformations of the shoulder, elbow and wrist modules respectively. It is assumed that the self-calibration process will enable precise computation of the forward kinematic transformations of the individual CDPM modules when their cable lengths are known.

III. CALIBRATION MODEL

The presence of geometric errors cause the nominal fixed transformation frames to shift to the actual frames (denoted by a superscript 'a'). Hence, the objective of the calibration model is to identify the errors between the nominal and actual frames, termed the calibrated frame (denoted by a superscript 'c'). Extending the approach adopted in [10], a calibration model is formulated using the POE formula

to represent the calibrated frames. While the other representations (i.e., D-H representation) result in complicated calibration models due to the highly coupled error parameters and suffer from formulation singularity, this is easily resolved by using POE. This is because it overcomes the issue of formulation singularity and a new local calibrated reference frame can be arbitrarily assigned. The kinematic errors in a fixed kinematic transformation can be treated as a twist, i.e., an element of $se(3)$. In addition, a twist has a 6-dimensional vector representation which simplifies the formulation (Refer to Appendix for details on the geometric background of rigid body kinematics).

According to the definition of matrix logarithm defined on $SE(3)$, there exists a $\hat{t} \in se(3)$ for a given $\mathbf{T} \in SE(3)$ such that $e^{\hat{t}} = T$. Hence, it is sufficient to let $e^{\hat{t}_{ij}} = T_{ij}$ and Eq. (1) is rewritten as:

$$\mathbf{T}_{OF} = e^{\hat{t}_{OB_s}}.\mathbf{T}_{B_sS}.e^{\hat{t}_{SB_e}}.\mathbf{T}_{B_eE}.e^{\hat{t}_{EB_w}}.\mathbf{T}_{B_wW}.e^{\hat{t}_{WF}} \tag{2}$$

Since the individual modules have undergone self-calibration, their transformation matrices (i.e., $\mathbf{T}_{B_sS}$, $\mathbf{T}_{B_eE}$ and $\mathbf{T}_{B_wW}$) are assumed to be computed with sufficient accuracy. Hence, any errors that may arise will be from the fixed forward kinematic transformations (i.e., $e^{\hat{t}_{OB_s}}$, $e^{\hat{t}_{SB_e}}$, $e^{\hat{t}_{EB_w}}$ and $e^{\hat{t}_{WF}}$) between the various CDPM modules attached serially to form the 7-DOF CDRA. Hence their kinematic errors are denoted by $\delta\hat{t}_{OB_s}$, $\delta\hat{t}_{SB_e}$, $\delta\hat{t}_{EB_w}$ and $\delta\hat{t}_{WF}$ respectively. Since $\hat{t}_{ij}$ belongs to $se(3)$, $\delta\hat{t}_{ij}$ will also belong to $se(3)$. Hence, $\delta e^{\hat{t}_{ij}} = \delta\hat{t}_{ij}.e^{\hat{t}_{ij}}$. Linearizing Eq. (2) results in:

$$\begin{aligned}\delta\mathbf{T}_{OF} &= \delta\hat{t}_{OB_S}.e^{\hat{t}_{OB_s}}.\mathbf{T}_{B_sS}.e^{\hat{t}_{SB_e}}.\mathbf{T}_{B_eE}.e^{\hat{t}_{EB_w}}.\mathbf{T}_{B_wW}.e^{\hat{t}_{WF}} \\ &+ e^{\hat{t}_{OB_s}}.\mathbf{T}_{B_sS}.\delta\hat{t}_{SB_e}.e^{\hat{t}_{SB_e}}.\mathbf{T}_{B_eE}.e^{\hat{t}_{EB_w}}.\mathbf{T}_{B_wW}.e^{\hat{t}_{WF}} \\ &+ e^{\hat{t}_{OB_s}}.\mathbf{T}_{B_sS}.e^{\hat{t}_{SB_e}}.\mathbf{T}_{B_eE}.\delta\hat{t}_{EB_w}.e^{\hat{t}_{EB_w}}.\mathbf{T}_{B_wW}.e^{\hat{t}_{WF}} \\ &+ e^{\hat{t}_{OB_s}}.\mathbf{T}_{B_sS}.e^{\hat{t}_{SB_e}}.\mathbf{T}_{B_eE}.e^{\hat{t}_{EB_w}}.\mathbf{T}_{B_wW}.\delta\hat{t}_{WF}.e^{\hat{t}_{WF}}\end{aligned} \tag{3}$$

Right-multiplying both sides of Eq. (3) with $\mathbf{T}_{OF}^{-1}$ results in:

$$\begin{aligned}\delta\mathbf{T}_{OF}.\mathbf{T}_{OF}^{-1} &= \delta\hat{t}_{OB_s} + \mathbf{T}_{OS}.\delta\hat{t}_{SB_e}.\mathbf{T}_{OS}^{-1} \\ &+ \mathbf{T}_{OE}.\delta\hat{t}_{EB_w}.\mathbf{T}_{OE}^{-1} + \mathbf{T}_{OW}.\delta\hat{t}_{WF}.\mathbf{T}_{OW}^{-1}\end{aligned} \tag{4}$$

Where:

$$\mathbf{T}_{OS} = e^{\hat{t}_{OB_s}}.\mathbf{T}_{B_sS}$$

$$\mathbf{T}_{OE} = e^{\hat{t}_{OB_s}}.\mathbf{T}_{B_sS}.e^{\hat{t}_{SB_e}}.\mathbf{T}_{B_eE}$$

$$\mathbf{T}_{OW} = e^{\hat{t}_{OB_s}}.\mathbf{T}_{B_sS}.e^{\hat{t}_{SB_e}}.\mathbf{T}_{B_eE}.e^{\hat{t}_{EB_w}}.\mathbf{T}_{B_wW}$$

The definition of the *matrix logarithm* and the *adjoint representation* of $SE(3)$ results in the following representations [11]:

$$\delta\mathbf{T}_{ij}.\mathbf{T}_{ij}^{-1} = \log[\mathbf{T}_{ij}^{a}.\mathbf{T}_{ij}^{-1}] \tag{5}$$

$$\mathbf{T}_{ij}.\delta\hat{t}_{jk}.\mathbf{T}_{ij}^{-1} = Ad_{T_{ij}}.\delta t_{jk} \tag{6}$$

Where $\mathbf{T}_{ij}^{a}$ is the actual (measured) transformation pose.

Hence, Eq. (4) is rewritten as:

$$\begin{aligned}\log[\mathbf{T}_{OF}^{a}.\mathbf{T}_{OF}^{-1}]^{V} &= \delta t_{OB_s} + Ad_{T_{OS}}.\delta t_{SB_e} \\ &+ Ad_{T_{OE}}.\delta t_{EB_w} + Ad_{T_{OW}}.\delta t_{WF}\end{aligned} \tag{7}$$

Where $\log[\mathbf{T}_{OF}^{a}.\mathbf{T}_{OF}^{-1}]^{V} \in \Re^{6\times1}$ is the vector representation of $\log[\mathbf{T}_{OF}^{a}.\mathbf{T}_{OF}^{-1}] \in se(3)$. Similarly, δt_{jk} is the 6-dimensional vector representation of $\delta\hat{t}_{jk} \in se(3)$. Geometrically, $\log[\mathbf{T}_{OF}^{a}.\mathbf{T}_{OF}^{-1}]^{V}$ represents the gross kinematic error of the tool-tip frame $\{K_F\}$ expressed in the world frame $\{K_O\}$. From Eq. (7), it is equal to the sum of kinematic errors in $\mathbf{T}_{OB_s}$, $\mathbf{T}_{SB_e}$, $\mathbf{T}_{EB_w}$ and $\mathbf{T}_{WF}$, also expressed in the world frame $\{K_O\}$. In each of the 6-dimensional error vectors, the first three parameters represent the position errors $(\delta x, \delta y, \delta z)$, while the remaining three represent the orientation errors $(\delta\theta_x, \delta\theta_y, \delta\theta_z)$. Eq. (7) is simplified into a linear calibration model as follows:

$$Y = D \cdot X \tag{8}$$

Where $Y = \log[\mathbf{T}_{OF}^{a}.\mathbf{T}_{OF}^{-1}]^{V} \in \Re^{6\times1}$, $D = [I_{6\times6} \quad Ad_{T_{OS}} \quad Ad_{T_{OE}} \quad Ad_{T_{OW}}] \in \Re^{6\times24}$ and $X = \{\delta t_{OB_s}{}^{T}, \delta t_{SB_e}{}^{T}, \delta t_{EB_w}{}^{T}, \delta t_{WF}{}^{T}\}^{T} \in \Re^{24\times1}$. $\mathbf{T}_{OF}^{a}$ is obtained by taking measurements using a coordinate measuring machine and a calibration block located at both frames $\{K_O\}$ and $\{K_F\}$. D is the calibration jacobian matrix that reflects the 24 kinematics error parameters (i.e., X) that exist in the whole system from Y. $\mathbf{T}_{OF}^{-1}$ and D are determined from the nominal kinematic model.

IV. CALIBRATION ALGORITHM

Based on the calibration model presented in Eq. (8), an iterative least-square algorithm is employed to determine the calibrated frames for the fixed forward kinematic transformation matrices $\mathbf{T}_{OB_s}$, $\mathbf{T}_{SB_e}$, $\mathbf{T}_{EB_w}$ and $\mathbf{T}_{WF}$. In order to obtain reliable results, it is required to take measurements at several poses. For m sets of measurement poses, the k^{th} pose with its set of tool-tip frame pose measurements will result in Y_k and its corresponding D_k. After m sets of measurement data, Y_k and D_k are stacked to form the following equation:

$$\widetilde{Y} = \widetilde{D} \cdot X \tag{9}$$

Where $\widetilde{Y} = \{Y_1{}^{T}, \ldots, Y_m{}^{T}\}^{T} \in \Re^{6m\times1}$ and $\widetilde{D} = \{D_1{}^{T}, \ldots, D_m{}^{T}\}^{T} \in \Re^{6m\times24}$. Since the model in Eq. (9) contains $6m$ linear equations with 24 variables, the least-squares algorithm is used (Note: Eq. (9) must have at least four measurement poses). The least-squares solution of X is given as:

$$X = (\widetilde{D}^{T}\widetilde{D})^{-1} \cdot \widetilde{D}^{T} \cdot \widetilde{Y} \tag{10}$$

Where $(\widetilde{D}^{T}\widetilde{D})^{-1}\widetilde{D}^{T}$ is the pseudo-inverse of $\widetilde{D}$. The solution of Eq. (10) is further improved through iterative substitution as shown in Fig. 4. A refinement in the least-squares algorithm is achieved by iterative looping. Once the kinematic error parameter vector, X is identified, $\mathbf{T}_{OB_s}$, $\mathbf{T}_{SB_e}$, $\mathbf{T}_{EB_w}$ and $\mathbf{T}_{WF}$ are updated after every loop k by substituting X into the following equations:

$$(\mathbf{T}_{OB_s})_{k+1} = e^{\hat{t}_{OB_s}}.(\mathbf{T}_{OB_s})_k \tag{11}$$

$$(\mathbf{T}_{SB_e})_{k+1} = e^{\hat{t}_{SB_e}}.(\mathbf{T}_{SB_e})_k \tag{12}$$

$$(\mathbf{T}_{EB_w})_{k+1} = e^{\hat{t}_{EB_w}}.(\mathbf{T}_{EB_w})_k \tag{13}$$

$$(\mathbf{T}_{WF})_{k+1} = e^{\hat{t}_{WF}}.(\mathbf{T}_{WF})_k \tag{14}$$

This procedure is repeated until the norm of the error vector $\|X\|$ approaches a certain tolerance limit, ε, which is close to zero. Then the final $\mathbf{T}_{OB_s}$, $\mathbf{T}_{SB_e}$, $\mathbf{T}_{EB_w}$ and $\mathbf{T}_{WF}$ represent the calibrated kinematic transformations, denoted by $\mathbf{T}^c_{OB_s}$, $\mathbf{T}^c_{SB_e}$, $\mathbf{T}^c_{EB_w}$ and $\mathbf{T}^c_{WF}$ respectively.

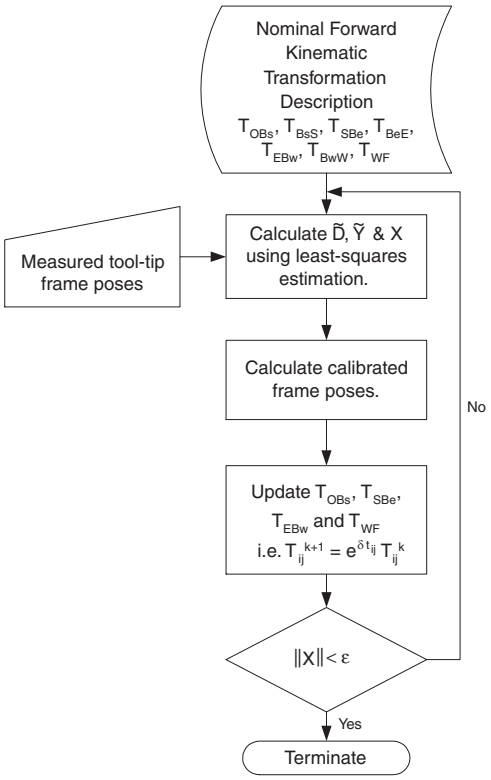

Fig. 4. Flowchart of the iterative calibration algorithm for the 7-DOF CDRA

After the iterative procedure, the kinematic error vector X does not represent the actual kinematic errors. Nevertheless, in order to compare the calibrated frame poses with their nominal frame poses, the actual kinematic errors is determined with the use of the matrix logarithm as follows:

$$\delta t_{OB_s} = \log[\mathbf{T}^c_{OB_s}.\mathbf{T}^{-1}_{OB_s}]^V \quad (15)$$

$$\delta t_{SB_e} = \log[\mathbf{T}^c_{SB_e}.\mathbf{T}^{-1}_{SB_e}]^V \quad (16)$$

$$\delta t_{EB_w} = \log[\mathbf{T}^c_{EB_w}.\mathbf{T}^{-1}_{EB_w}]^V \quad (17)$$

$$\delta t_{WF} = \log[\mathbf{T}^c_{WF}.\mathbf{T}^{-1}_{WF}]^V \quad (18)$$

After the calibration procedure, the forward kinematic equation becomes:

$$\mathbf{T}^c_{OF} = \mathbf{T}^c_{OB_s}.\mathbf{T}_{B_sS}.\mathbf{T}^c_{SB_e}.\mathbf{T}_{B_eE}.\mathbf{T}^c_{EB_w}.\mathbf{T}_{B_wW}.\mathbf{T}^c_{WF} \quad (19)$$

In order to evaluate the calibration result, two deviation metrics between the actual (measured) 'a' and calibrated 'c' tool-tip frames are mathematically defined as [10]:

$$\delta p = \sqrt{\frac{1}{m}\sum_{k=1}^{m}(P_{ak}-P_{ck})^T.(P_{ak}-P_{ck})} \quad (20)$$

$$\delta R = \sqrt{\frac{1}{m}\sum_{k=1}^{m}\left(\log(R^{-1}_{ak}R_{ck})^V\right)^T\left(\log(R^{-1}_{ak}R_{ck})^V\right)} \quad (21)$$

Where δp and δR denote the average quantified position and orientation deviation metrics respectively, between the calibrated and actual poses of the tool-tip frame.

V. COMPUTER SIMULATION

In this section, computer simulation studies were carried out on the 7-DOF CDRA with the optimized individual CDPM modules. This is to demonstrate the accuracy and robustness of the calibration algorithm. The simulation will investigate the effect of kinematic errors under noise-free measurements. The units of the kinematic parameters are in *radians* and *millimeters*. For the simulation studies, the following procedure is employed:

1) Generate two sets of m random shoulder, elbow and wrist module poses, i.e., $\mathbf{T}_{B_sS}$, $\mathbf{T}_{B_eE}$ and $\mathbf{T}_{B_wW}$ respectively (within the limits of the mechanical joints motion range and satisfying tension-closure condition). One set will be used for calibration while the other will be used for verification.

2) Assign kinematic errors in the nominal poses of $\mathbf{T}_{OB_s}$, $\mathbf{T}_{SB_e}$, $\mathbf{T}_{EB_w}$ and $\mathbf{T}_{WF}$ by introducing $\delta t'_{OB_s}$, $\delta t'_{SB_e}$, $\delta t'_{EB_w}$ and $\delta t'_{WF}$ respectively.

3) Using the generated set of random poses in Step 1, calculate the two m sets of 'simulated' actual tool-tip frame poses based on:

$$\mathbf{T}^a_{OF} = \mathbf{T}^a_{OB_s}.\mathbf{T}_{B_sS}.\mathbf{T}^a_{SB_e}.\mathbf{T}_{B_eE}.\mathbf{T}^a_{EB_w}.\mathbf{T}_{B_wW}.\mathbf{T}^a_{WF}$$

Where:

$$\mathbf{T}^a_{OB_s} = e^{\hat{t'}_{OB_s}}.\mathbf{T}_{OB_s}$$

$$\mathbf{T}^a_{SB_e} = e^{\hat{t'}_{SB_e}}.\mathbf{T}_{SB_e}$$

$$\mathbf{T}^a_{EB_w} = e^{\hat{t'}_{EB_w}}.\mathbf{T}_{EB_w}$$

$$\mathbf{T}^a_{WF} = e^{\hat{t'}_{WF}}.\mathbf{T}_{WF}$$

4) Identify the preset kinematic errors using the calibration algorithm and the first set of m 'simulated' actual tool-tip frame pose measurements.

5) Verify the calibrated poses $\mathbf{T}^c_{OB_s}$, $\mathbf{T}^c_{SB_e}$, $\mathbf{T}^c_{EB_w}$ and $\mathbf{T}^c_{WF}$ (based on Eq. (19)) using the second set of m 'simulated' actual tool-tip frame pose measurements.

The theoretical lower bound for the number of measured poses is four but for accuracy and robustness, it is set to five. From the viewpoint of computer simulation, the kinematic errors $\{\delta x', \delta y', \delta z'\}$ (i.e., position) and $\{\delta\theta'_x, \delta\theta'_y, \delta\theta'_z\}$ (i.e., orientation) are randomly generated with uniformly distributed deviations of $\pm d_\upsilon$ and $\pm d_\omega$. From the simulation results, injected errors with uniformly distributed deviations of $d_\upsilon = 1$ *mm* and $d_\omega = 0.05$ *rad* are recoverable within three to four iterations. This demonstrates the accuracy of the calibration model for the 7-DOF cable-driven robotic

arm. From Table I, the preset kinematic errors are well-recovered although the preset errors are significantly large. Results shown in Fig. 5 further reinforce the effectiveness of the calibration model, where both deviation metrics δp and δR (given in Eqs. (20) and (21)) are driven to approximately zero values within three iterations.

TABLE I

PRESET AND IDENTIFIED KINEMATIC ERRORS IN THE 'SIMULATED' CALIBRATION OF THE 7-DOF CDRA

$\delta t'_{ij}$	Preset Kinematic Errors	Identified Kinematic Errors
$\delta t'_{OB_s}$	$\{-6.5597, 3.8277, 8.9030, 0.1207, 0.1538, -0.0910\}^T$	$\{-6.5597, 3.8277, 8.9030, 0.1207, 0.1538, -0.0910\}^T$
$\delta t'_{SB_e}$	$\{2.0158, 6.4144, 6.0300, -0.1290, 0.0207, -0.0010\}^T$	$\{1.5354, 6.1907, 6.0510, -0.1290, 0.0223, -0.0011\}^T$
$\delta t'_{EB_w}$	$\{4.8284, 4.6296, 3.9088, 0.1285, -0.1471, 0.0130\}^T$	$\{4.8264, 4.8539, 3.8983, 0.1285, -0.1487, 0.0131\}^T$
$\delta t'_{WF}$	$\{6.1681, 3.6960, 5.2650, 0.1712, -0.0511, -0.0579\}^T$	$\{6.1681, 3.6960, 5.2650, 0.1712, -0.0511, -0.0579\}^T$

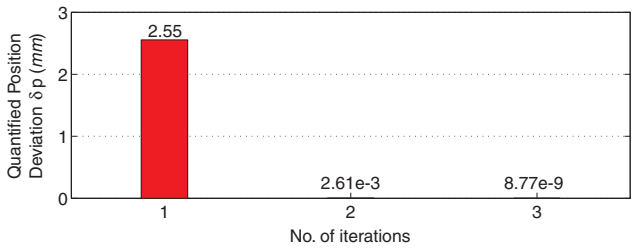

(a) Quantified position deviation metric convergence plot

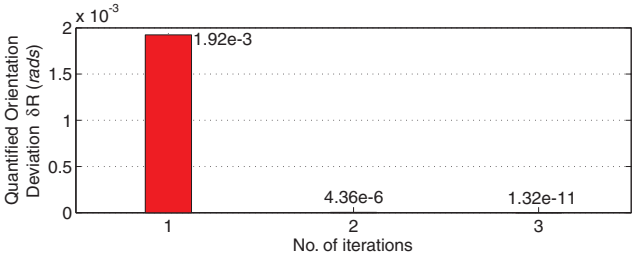

(b) Quantified orientation deviation metric convergence plot

Fig. 5. Calibration convergence plot for the 7-DOF CDRA using the 'simulated' set of pose measurements ($d_v = 1$ *mm* and $d_\omega = 0.05$ *rad*)

VI. EXPERIMENTAL RESULTS

In this section, experimental studies were carried out on the 7-DOF CDRA research prototype. This is to investigate the robustness of the calibration algorithm in practical applications with the existence of measurement noise. The experimental procedure is similar to the computer simulation procedure except that the tool-tip frame pose measurements are obtained using a coordinate measuring machine (from FARO with an accuracy of 80 μm) and a calibration block located at the tool-tip of the CDRA (see Fig. 6).

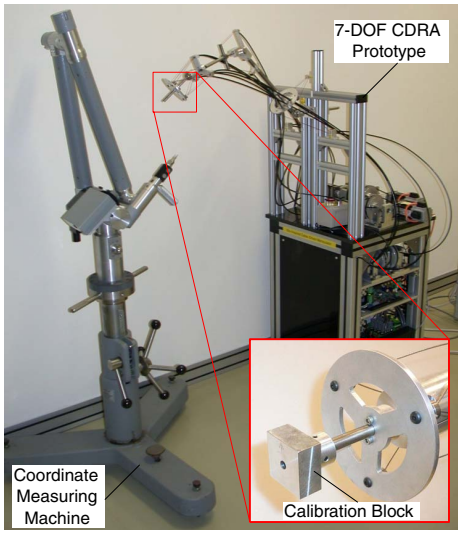

Fig. 6. Calibration experimental setup for the 7-DOF CDRA with the FARO coordinate measuring machine and calibration block

From this experimental study, deviation metrics δp and δR became relatively stable after greater than 15 tool-tip measurement poses (see Fig. 7). A full recovery of the errors in the fixed forward kinematic transformations is impossible, limited by the accuracy of the measurement device and the cable actuation unit. However, partial error recovery can be achieved and the proposed calibration model is able to accurately and robustly identify the errors in the nominal fixed forward kinematic transformations.

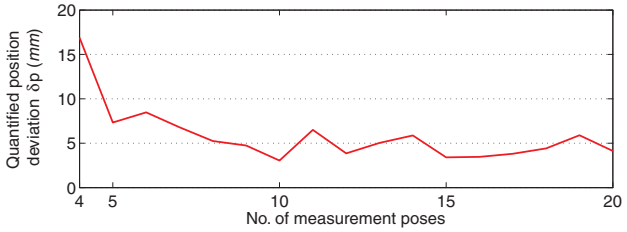

(a) Quantified position deviation metric convergence plot

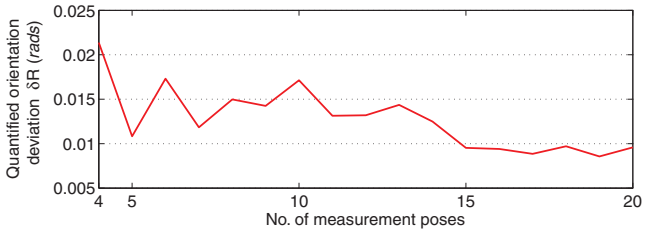

(b) Quantified orientation deviation metric convergence plot

Fig. 7. Calibration deviation metrics convergence plot for the 7-DOF CDRA using the 'experimental' set of tool-tip measurement poses

VII. CONCLUSION

For the 7-DOF self-calibrated modular cable-driven robotic arm, an effective calibration model is formulated based on the local POE formula and the measurement residue errors in the tool-tip frame pose measurements. This is to account

for any kinematic errors that might arise when serially assembling the individual self-calibrated CDPM modules to form the overall 7-DOF CDRA. A least-squares algorithm is employed to solve the calibration results iteratively due to the linear nature of the calibration model. Computer simulation studies were carried out to verify the algorithm. Simulation studies demonstrate that the preset kinematic errors in the complete arm assembly of up to ± 1 *mm* (for position) and ± 0.05 *rad* (for orientation), are fully recovered under noise-free measurement conditions. Under experimental conditions, the noise in measurements prevent full recovery of errors but nonetheless, these errors are precisely recovered with a minimum of 15 measurement poses. Hence this calibration model is able to accurately and robustly calibrate the 7-DOF CDRA.

APPENDIX: GEOMETRIC BACKGROUND

In kinematic analysis of rigid body motions, the *Special Euclidean Group*, or $SE(3)$, is commonly used to describe the configuration of a rigid body with regards to certain coordinate frames. If $\{K_A\}$ is a fixed inertial coordinate frame and $\{K_B\}$ is a body-attached coordinate frame, the configuration of $\{K_B\}$ with respect to $\{K_A\}$ is expressed either as an ordered pair or a 4×4 homogeneous matrix:

$$\mathbf{T}_{ab} = (\mathbf{p}_{ab}, \mathbf{R}_{ab}) = \begin{bmatrix} \mathbf{R}_{ab} & \mathbf{p}_{ab} \\ 0 & 1 \end{bmatrix} \tag{22}$$

Where $\mathbf{R}_{ab} \in SO(3)$ is the rigid body rotation of $\{K_B\}$ with respect to $\{K_A\}$ and $\mathbf{p}_{ab} \in \Re^{3\times 1}$ is the initial location of the origin of $\{K_B\}$ with respect to $\{K_A\}$. Note that $SO(3)$ or *Special Orthogonal Group*, refers to the 3×3 rotation matrices group. The group operation on $SE(3)$ allows the configuration of a frame $\{K_C\}$ to be described with respect to $\{K_A\}$ via an intermediate frame $\{K_B\}$ as $\mathbf{T}_{ac} = \mathbf{T}_{ab}.\mathbf{T}_{bc} = (\mathbf{p}_{ab}, \mathbf{R}_{ab}).(\mathbf{p}_{bc}, \mathbf{R}_{bc}) = (\mathbf{p}_{ab} + \mathbf{R}_{ab}.\mathbf{p}_{bc}, \mathbf{R}_{ab}.\mathbf{R}_{bc})$.

Since $SE(3)$ is a Lie Group, the *Lie Algebra* of $SE(3)$, denoted by $se(3)$, consists of matrices in the form:

$$\widehat{\$} = \begin{bmatrix} \widehat{\omega} & \upsilon \\ 0 & 0 \end{bmatrix} \tag{23}$$

Where $\widehat{\omega}$ is a 3×3 real skew-symmetric matrix which forms the Lie algebra of $SO(3)$, denoted by $so(3)$, and $\upsilon \in \Re^{3\times 1}$. An element of $\widehat{\omega} \in so(3)$ is regarded as a vector $\omega \in \Re^{3\times 1}$, while an element of $se(3)$ is represented as a 6×1 vector $\$ = (\upsilon, \omega) \in \Re^{6\times 1}$, termed as a *twist*. Interpreted using the theory of screws, a twist describes a general rigid body motion, simultaneously rotating and translating about a screw axis. ω is the unit directional vector of the screw axis and υ is the position of the screw axis relative to the origin.

An element of a Lie group can also be identified with a linear mapping between its Lie algebra via its *adjoint* representation, denoted by the symbol Ad. Suppose $\mathbf{T}_{ab}$ is a matrix Lie group with Lie algebra t. For every $X \in \mathbf{T}_{ab}$, the adjoint mapping $Ad_X : t \to t$ is defined by $Ad_X(V) = XVX^{-1}$ for $V \in t$. If $X = (\mathbf{p}_{ab}, \mathbf{R}_{ab})$ is an element of $SE(3)$, then its adjoint map acting on an element $V = (\upsilon_{ab}, \omega_{ab})$ of $se(3)$ is described as either:

$$Ad_X(V) = (\mathbf{p}_{ab} \times \mathbf{R}_{ab}\omega_{ab} + \mathbf{R}_{ab}\upsilon_{ab}, \mathbf{R}_{ab}\omega_{ab}) \tag{24}$$

Or its 6×6 matrix representation:

$$Ad_X(V) = \begin{bmatrix} \mathbf{R}_{ab} & \widehat{\mathbf{p}}_{ab}\mathbf{R}_{ab} \\ 0 & \mathbf{R}_{ab} \end{bmatrix} \begin{bmatrix} \upsilon_{ab} \\ \omega_{ab} \end{bmatrix} \tag{25}$$

An important relation between a Lie group, $SE(3)$, and its Lie algebra, $se(3)$ is the exponential mapping, defined on each Lie algebra. By letting $\widehat{s} \in se(3)$ $(s = (\upsilon, \omega))$ and $\|\omega\|^2 = \omega_x^2 + \omega_y^2 + \omega_z^2$, the exponential mapping is described as:

$$e^{\widehat{s}} = \begin{bmatrix} e^{\widehat{\omega}} & A\upsilon \\ 0 & 1 \end{bmatrix} \in SE(3) \tag{26}$$

Where $e^{\widehat{\omega}} = I + \frac{\sin\|\omega\|}{\|\omega\|}\widehat{\omega} + \frac{1-\cos\|\omega\|}{\|\omega\|^2}\widehat{\omega}^2$ and $A = I + \frac{1-\cos\|\omega\|}{\|\omega\|^2}\widehat{\omega} + \frac{\|\omega\|-\sin\|\omega\|}{\|\omega\|^2}\widehat{\omega}^2$.

The matrix logarithm also establishes a relation between a Lie group and its Lie algebra, while the Lie group is in the neighborhood of the identity. By letting $\mathbf{R}_{ab} \in SO(3)$ such that $\text{trace}(\mathbf{R}_{ab}) \neq 1$, $1 + 2\cos\phi = \text{trace}(\mathbf{R}_{ab})$, and $\|\phi\| < \pi$, the matrix logarithm is described as:

$$\log \begin{bmatrix} \mathbf{R}_{ab} & \mathbf{p}_{ab} \\ 0 & 1 \end{bmatrix} = \begin{bmatrix} \widehat{\omega} & A^*\mathbf{p}_{ab} \\ 0 & 0 \end{bmatrix} \in se(3) \tag{27}$$

Where $\widehat{\omega} = \log\mathbf{R}_{ab} = \frac{\phi}{2\sin\phi}(\mathbf{R}_{ab} - \mathbf{R}_{ab}^T)$ and $A^* = I - \frac{1}{2}\widehat{\omega} + \frac{2\sin\|\omega\| - \|\omega\|(1+\cos\|\omega\|)}{2\|\omega\|^2\sin\|\omega\|}\widehat{\omega}^2$. If ϕ is very small, the $\widehat{\omega} \approx \frac{(\mathbf{R}_{ab} - \mathbf{R}_{ab}^T)}{2}$.

(Refer to [12] for more details on Lie group rigid body kinematics.)

ACKNOWLEDGMENT

S.K. Mustafa would like to thank the Agency for Science, Technology & Research for awarding his PhD scholarship. The authors would also like to thank Prof I-Ming Chen from the School of MAE, NTU.

REFERENCES

[1] Y. Sodeyama, I. Mizuuchi, T. Yoshikai, Y. Nakanishi, and M. Inaba, "A shoulder structure of muscle-driven humanoid with shoulder blades," in *Proceedings of IEEE/RJS International Conference on Intelligent Robots and Systems*, pp. 1077–1082, Edmonton, Canada, 2005.

[2] R. M. Alqasemi, E. McCaffrey, K. Edwards, and R. Dubey, "Analysis, evaluation and development of wheelchair-mounted robotics arms," in *Proceedings of IEEE International Conference on Rehabilitation Robotics*, pp. 469–472, Chicago, USA, 2005.

[3] J. Choi, J. Kim, D. Kim, C. Lee, J.-T. Park, and J.-O. Park, "Design and characteristic analysis of a 7-dof hybrid master arm with human kinematics," in *Proceedings of ASME Dynamic Systems and Control Division*, pp. 195–205, 1998.

[4] L. Zollo, C. Laschi, G. Teti, B. Siciliano, and P. Dario, "Functional compliance in the control of a rehabilitation robot," in *Proceedings of IEEE/RSJ International Conference on Intelligent Robots and Systems*, pp. 2221–2226, Maui, Hawaii, 2001.

[5] G. Yang, H. L. Ho, W. Chen, W. Lin, and M.S. Kurbanhusen, "A haptic device wearable on a human arm," in *Proceedings of IEEE Conference on Robotics, Automation and Mechatronics*, pp. 243–248, Singapore, 2004.

[6] G. Yang, W. Lin, M.S. Kurbanhusen, C.B. Pham, and S.H. Yeo, "Kinematic design of a 7-dof cable-driven humanoid arm: A solution-in-nature approach," in *Proceedings of IEEE/ASME Advanced Intelligent Mechatronics*, pp. 444–449, Monterey, California, USA, 2005.

[7] B. Mooring, Z. Roth, and M. Driels, *Fundamentals of Manipulator Calibration*. John Wiley & Sons, Inc., 1991.

[8] S.K. Mustafa, G. Yang, S.H. Yeo, W. Lin, and I.-M. Chen, "Self-calibration of a biologically-inspired 7-DOF cable-driven robotic arm," *IEEE/ASME Transactions on Mechatronics*, (to appear in vol. 13 no. 1, 2008).

[9] H. Zhuang, Z.S. Roth, and R. Sudhakar, "Simultaneous robot/world and tool/flange calibration by solving homogeneous transformation equations of the form AX=YB," *IEEE Transactions on Robotics and Automation*, vol. 10, no. 4, pp. 549–554, 1994.

[10] G. Yang, I.-M. Chen, S.H. Yeo, and W.K. Lim, "Simultaneous base and tool calibration for self-calibrated parallel robots," *Robotica*, vol. 20, no. 4, pp. 367–374, 2002.

[11] F.C. Park, "Computational aspect of manipulators via product of exponential formula for robot kinematics", *IEEE Transactions on Automatic Control*, vol. 39, no. 9, pp. 643-647, 1994.

[12] J.M. Selig, *Geometric Fundamentals of Robotics*, Springer, 2005.